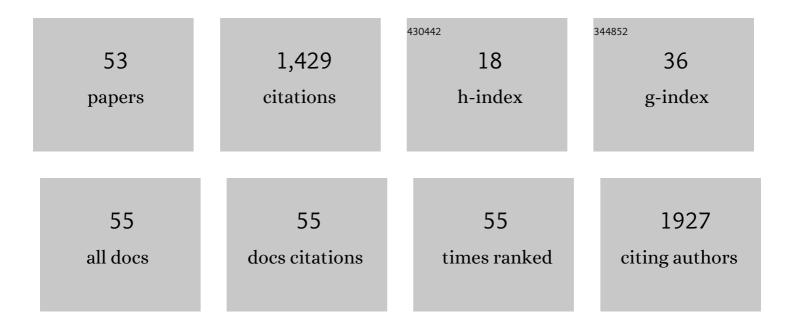
Shuhang Chen

List of Publications by Year in descending order

Source: https://exaly.com/author-pdf/6610796/publications.pdf Version: 2024-02-01



#	Article	IF	CITATIONS
1	Low-dose real-time X-ray imaging with nontoxic double perovskite scintillators. Light: Science and Applications, 2020, 9, 112.	7.7	272
2	PET image denoising using unsupervised deep learning. European Journal of Nuclear Medicine and Molecular Imaging, 2019, 46, 2780-2789.	3.3	157
3	Thermally activated delayed fluorescence (TADF) organic molecules for efficient X-ray scintillation and imaging. Nature Materials, 2022, 21, 210-216.	13.3	146
4	Rapid image deconvolution and multiview fusion for optical microscopy. Nature Biotechnology, 2020, 38, 1337-1346.	9.4	105
5	Direct delineation of myocardial infarction without contrast agents using a joint motion feature learning architecture. Medical Image Analysis, 2018, 50, 82-94.	7.0	96
6	Simultaneous multiview capture and fusion improves spatial resolution in wide-field and light-sheet microscopy. Optica, 2016, 3, 897.	4.8	53
7	Sparse representation and dictionary learning penalized image reconstruction for positron emission tomography. Physics in Medicine and Biology, 2015, 60, 807-823.	1.6	41
8	Deep reconstruction model for dynamic PET images. PLoS ONE, 2017, 12, e0184667.	1.1	40
9	Changes in Topological Organization of Functional PET Brain Network with Normal Aging. PLoS ONE, 2014, 9, e88690.	1.1	37
10	Meshfree implementation of individualized active cardiac dynamics. Computerized Medical Imaging and Graphics, 2010, 34, 91-103.	3.5	36
11	Untwisting the Caenorhabditis elegans embryo. ELife, 2015, 4, .	2.8	33
12	Using MicroPET Imaging in Quantitative Verification of the Acupuncture Effect in Ischemia Stroke Treatment. Scientific Reports, 2013, 3, 1070.	1.6	31
13	A Meshfree Representation for Cardiac Medical Image Computing. IEEE Journal of Translational Engineering in Health and Medicine, 2018, 6, 1-12.	2.2	30
14	FBP-Net for direct reconstruction of dynamic PET images. Physics in Medicine and Biology, 2020, 65, 235008.	1.6	30
15	Training on Abacus-Based Mental Calculation Enhances Visuospatial Working Memory in Children. Journal of Neuroscience, 2019, 39, 6439-6448.	1.7	29
16	Modular segregation of task-dependent brain networks contributes to the development of executive function in children. NeuroImage, 2020, 206, 116334.	2.1	28
17	Physiome-Model–Based State-Space Framework for Cardiac Deformation Recovery. Academic Radiology, 2007, 14, 1341-1349.	1.3	21
18	State-Space Analysis of Cardiac Motion With Biomechanical Constraints. IEEE Transactions on Image Processing, 2007, 16, 901-917.	6.0	19

SHUHANG CHEN

#	Article	IF	CITATIONS
19	Simultaneous Reconstruction and Segmentation of Dynamic PET via Low-Rank and Sparse Matrix Decomposition. IEEE Transactions on Biomedical Engineering, 2015, 62, 1784-1795.	2.5	19
20	Automated Detection Framework of the Calcified Plaque with Acoustic Shadowing in IVUS Images. PLoS ONE, 2014, 9, e109997.	1.1	17
21	Populational and individual information based PET image denoising using conditional unsupervised learning. Physics in Medicine and Biology, 2021, 66, 155001.	1.6	15
22	Blip upâ€down acquisition for spin―and gradientâ€echo imaging (<scp>BUDAâ€SAGE</scp>) with selfâ€supervised denoising enables efficient <scp>T₂</scp> , <scp>T₂</scp> *, para―and diaâ€magnetic susceptibility mapping. Magnetic Resonance in Medicine, 2022, 88, 633-650.	1.9	15
23	Separation of a Mixture of Simultaneous Dual-Tracer PET Signals: A Data-Driven Approach. IEEE Transactions on Nuclear Science, 2017, 64, 2588-2597.	1.2	13
24	A Genetically Encoded Biosensor Strategy for Quantifying Non-muscle Myosin II Phosphorylation Dynamics in Living Cells and Organisms. Cell Reports, 2018, 24, 1060-1070.e4.	2.9	13
25	Efficient T ₂ mapping with blipâ€up/down EPI and gSliderâ€SMS (T ₂ â€BUDAâ€gSlider). Magnetic Resonance in Medicine, 2021, 86, 2064-2075.	1.9	13
26	Robust recovery of myocardial kinematics using dual â"‹ â^ž \$mathcal {H}_{infty }\$ criteria. Multimedia Tools and Applications, 2018, 77, 23043-23071.	2.6	10
27	Multimodality Attention-Guided 3-D Detection of Nonsmall Cell Lung Cancer in ¹⁸ F-FDG PET/CT Images. IEEE Transactions on Radiation and Plasma Medical Sciences, 2022, 6, 421-432.	2.7	8
28	Cardiac MRI segmentation with focal loss constrained deep residual networks. Physics in Medicine and Biology, 2021, 66, .	1.6	8
29	Rapid high-quality PET Patlak parametric image generation based on direct reconstruction and temporal nonlocal neural network. NeuroImage, 2021, 240, 118380.	2.1	8
30	Low Dose PET Image Reconstruction with Total Variation Using Alternating Direction Method. PLoS ONE, 2016, 11, e0166871.	1.1	7
31	Nonlocal total variation based dynamic PET image reconstruction with low-rank constraints. Physica Scripta, 2019, 94, 065202.	1.2	7
32	3D Tensor Based Nonlocal Low Rank Approximation in Dynamic PET Reconstruction. Sensors, 2019, 19, 5299.	2.1	7
33	Robust Framework for PET Image Reconstruction Incorporating System and Measurement Uncertainties. PLoS ONE, 2012, 7, e32224.	1.1	6
34	Efficient knowledge distillation for liver CT segmentation using growing assistant network. Physics in Medicine and Biology, 2021, 66, 235005.	1.6	6
35	Joint reconstruction of dynamic PET activity and kinetic parametric images using total variation constrained dictionary sparse coding. Inverse Problems, 2017, 33, 055011.	1.0	5
36	Simultaneous estimation and segmentation from projection data in dynamic PET. Medical Physics, 2019, 46, 1245-1259.	1.6	5

SHUHANG CHEN

#	Article	IF	CITATIONS
37	Imaging mitochondrial complex I activation during a vibrotactile stimulation: A PET study using [18F]BCPP-EF in the conscious monkey brain. Journal of Cerebral Blood Flow and Metabolism, 2020, 40, 2521-2532.	2.4	4
38	Reconstruction for 3D PET Based on Total Variation Constrained Direct Fourier Method. PLoS ONE, 2015, 10, e0138483.	1.1	3
39	Nonlocal Low-Rank and Total Variation Constrained PET Image Reconstruction. , 2018, , .		3
40	Topological Charge Detection Using Generalized Contour-Sum Method from Distorted Donut-Shaped Optical Vortex Beams: Experimental Comparison of Closed Path Determination Methods. Applied Sciences (Switzerland), 2019, 9, 3956.	1.3	3
41	Spatio-temporal multi-task network cascade for accurate assessment of cardiac CT perfusion. Medical Image Analysis, 2021, 74, 102207.	7.0	3
42	Nonâ€invasive reconstruction of dynamic myocardial transmembrane potential with graphâ€based total variation constraints. Healthcare Technology Letters, 2019, 6, 181-186.	1.9	3
43	Medical image segmentation with generative adversarial semi-supervised network. Physics in Medicine and Biology, 2021, 66, 245008.	1.6	3
44	Unsupervised arterial spin labeling image superresolution via multiscale generative adversarial network. Medical Physics, 2022, 49, 2373-2385.	1.6	3
45	Cycle-consistent learning-based hybrid iterative reconstruction for whole-body PET imaging. Physics in Medicine and Biology, 2022, 67, 085016.	1.6	3
46	Sparse/Low Rank Constrained Reconstruction for Dynamic PET Imaging. PLoS ONE, 2015, 10, e0142019.	1.1	2
47	Quasi-plane shear wave propagation induced by acoustic radiation force with a focal line region: a simulation study. Australasian Physical and Engineering Sciences in Medicine, 2016, 39, 187-197.	1.4	2
48	Using MicroPET Imaging in Quantitative Verification of Acupuncture Effect in Ischemia Stroke Treatment. Nature Precedings, 2010, , .	0.1	1
49	Simultaneous reconstruction and segmentation of MRI image by manifold learning. , 2019, , .		1
50	Invertible AC-flow: Direct Attenuation Correction Of Pet Images Without Ct Or Mr Images. , 2022, , .		1
51	Liver-Buda-Sage: Simultaneous Whole Liver T ₂ and T* ₂ Mapping in one Breath-Hold. , 2022, , .		1
52	Nonlinear Dual Reconstruction of SPECT Activity and Attenuation Images. PLoS ONE, 2014, 9, e106951.	1.1	0
53	Improved Patlak Reconstruction from Low-dose Dynamic PET Using Temporal Non-local Neural Network. , 2020, , .		0